Environmental Science Processes & Impacts

ROYAL SOCIETY OF CHEMISTRY

PAPER

View Article Online
View Journal | View Issue

Check for updates

Cite this: *Environ. Sci.: Processes Impacts*, 2025, **27**, 1704

Indoor surface chemistry variability: microspectroscopic analysis of deposited particles in dwellings across the United States†

Alison M. Fankhauser, [a] Jana L. Butman, [b] Madeline E. Cooke, [a] Yekaterina Fyodorova,[a] Yangdongling Liu,[b] Rachel E. O'Brien, [cd] V. Faye McNeill, *[ef] Franz M. Geiger, *[b] Vicki H. Grassian *[g] and Andrew P. Ault *[a]

Received 30th December 2024
Accepted 25th February 2025

DOI: 10.1039/d4em00816b

rsc.li/espi

Dwellings across the United States range dramatically with respect to numerous variables (*e.g.*, size, ventilation, and proximity to outdoor sources), and there are considerable uncertainties regarding the heterogeneity in chemical composition and physical properties of indoor particles and surfaces. Stay-at-home orders early in the COVID-19 pandemic led to significant portions of the population spending high fractions of their time at their primary dwelling. Stay-at-HomeChem leveraged a network of indoor chemistry researchers to study indoor air quality and surface chemistry in their homes (March–April 2020). Within this effort, glass microscope slides were deployed in kitchens and other rooms in dwellings across the country for time periods ranging from as short as three hours up to three weeks. Overall, results from 10 occupied homes (15 distinct rooms) showed that collected material on this time scale was primarily deposited particles, rather than thick films, based on optical microscopy and profilometry. Raman microspectroscopy and optical photothermal infrared (O-PTIR) spectroscopy showed that organic modes were dominant, including ν(C–H), δ(C–H), and ν(C=O), with minimal contributions from inorganic ions commonly observed in outdoor particulate matter (sulfate, nitrate, or ammonium). Spectral variability within the C–H stretching and fingerprint regions demonstrate differing compositions of deposited particles, often related to cooking activities (*e.g.*, organic particles from cooking oils). Differences within a single dwelling, highlighted that particles from cooking were key contributors in some other rooms, but not all, reinforcing that sources and ventilation likely led to quite distinct surfaces in different rooms. Overall, these results demonstrate the need for real-world measurements to assess the representativeness of assumptions regarding exposure to organic material indoors.

Environmental significance

Surfaces within dwellings play a key role in controlling indoor exposures to pollutants, but are challenging to define and characterize due to the wide variability in sources and indoor environments across housing types and regions with different climates. This study analyzed samples collected within occupied dwellings during the early SARS-CoV-2 pandemic period to improve understanding of the nature of indoor surfaces, including the relative importance of particle deposition *versus* secondary organic film growth on the time-scale of these studies (weeks). Distinct chemical and morphological differences were observed between and within dwellings, with kitchens having the most surface-collected and chemically-distinct material. These findings provide important information for indoor chemistry models to consider when predicting multiphase chemistry, semi-volatile partitioning, and inhalation exposure.

[a]*Department of Chemistry, University of Michigan, Ann Arbor, Michigan 48109, USA. E-mail: aulta@umich.edu*

[b]*Department of Chemistry, Northwestern University, 2145 Sheridan Road, Evanston, Illinois 60660, USA. E-mail: f-geiger@northwestern.edu*

[c]*Department of Chemistry, William & Mary, Williamsburg, Virginia 23185, USA*

[d]*Department of Civil and Environmental Engineering, University of Michigan, Ann Arbor, Michigan 48109, USA*

[e]*Department of Chemical Engineering, Columbia University, New York, New York 10027, USA. E-mail: vfm2103@columbia.edu*

[f]*Department of Earth and Environmental Sciences, Columbia University, New York, New York 10027, USA*

[g]*Department of Chemistry and Biochemistry, University of California, San Diego, La Jolla, CA, USA. E-mail: vhgrassian@ucsd.edu*

† Electronic supplementary information (ESI) available. See DOI: https://doi.org/10.1039/d4em00816b

Introduction

While much emphasis has been placed on improving ambient air quality over the past several decades, it is worth noting that under some circumstances, indoor air can be even more polluted than that outdoors.[1,2] Americans spend roughly 90% of their lifetime indoors,[3] whether at their homes, schools, or work, making indoor environments a key location for exposure to air pollution in the form of inhaled particles and gases. A great deal has already been learned about indoor air[4,5] in particular due to collaborative campaigns that have studied how human activities and other perturbations influence chemical compounds within a home.[6–8] Specifically, the House Observations of Microbial and Environmental Chemistry (HOMEChem) study investigated how cooking, cleaning, and occupancy affected air and surface chemistry within a test house.[9] Surfaces have been shown to be important for indoor air quality because of the high surface area to volume ratios indoors (~2–5 m^2 m^{-3})[10–14] relative to outdoors (~0.01 m^2 m^{-3}).[10,11] This high surface area leads indoor surfaces to serve as both reservoirs for various compounds[12,15] as well as sites for multiphase reactions.[16–18] The HOMEChem campaign provided further evidence of the complexity and importance of surfaces for indoor air chemistry.[19,20]

Within indoor chemistry research two somewhat distinct research directions have evolved regarding indoor surfaces.[18,21] In one direction, information regarding surfaces as reservoirs or sites for reactions focuses on extractions or inferences from gas phase measurements. Wang *et al.*[12] found that a range of common indoor air contaminants predominantly resided in surface reservoirs and participated in rapid gas-surface partitioning. Furthermore, Lunderberg, *et al.*[22] showed that semi-volatile organic compound (SVOC) emissions from these condensed-phase surface reservoirs contributed to organic particulate matter during primary particle emission events. In particular, O'Brien *et al.*[19] reported that surface films collected in a test kitchen were chemically similar to cooking organic aerosol, but contained larger, more oxidized molecules. This type of analysis provides information about molecular species present on surfaces, but provides minimal information about the physical properties of the surface (*e.g.*, fractional coverage, morphology, roughness, *etc.*).

The second indoor chemistry research direction has focused on directly measuring the physicochemical properties of the surface.[18] Specifically considering glass surfaces in the HOMEChem campaign, Or *et al.*[20] demonstrated that submicron particle deposition from cooking events substantially contributed to the organic material accumulation, dominating the volume loadings, and affected the morphology and chemistry of the surface. However, these one-day samples had uneven topography, showing a coexistence of coated and bare glass surface, which adds complexity when trying to accurately model surface deposition. This built upon previous work in which Or *et al.*[23] showed particle deposition and surface film formation increased the surface area and roughness of glass surfaces over the course of six months in a variety of indoor locations. The kitchen had the most accumulation of material, but even on this long timescale, the surface films for all room types were not homogenous and did not completely cover the surface, highlighting the heterogeneity of indoor surfaces.

While previous work has primarily sampled in the kitchens of designed test homes, it is important to understand the composition of indoor deposition in real-world, occupied dwellings. Furthermore, previous studies have focused on bulk mass spectrometry[24–26] with only a few studies using microscopy-based analyses.[20,23] However, microscopy-based Raman and O-PTIR spectroscopies have demonstrated their potential to provide further insights into surface properties and behavior. Herein, we show example Raman and O-PTIR spectra and surface imaging for occupied households from a range of geographic locations.

Methods

Sampling

The sampling approach was based on previously reported methods[23,27] for in-home collection of primary and secondary material on passive samplers, but at a level of sophistication commensurate with the available materials during the early stages of the shutdown. Briefly, glass microscope slides were cleaned using methanol and placed vertically using a holder in a chosen room in homes located across the continental United States. A cover slide was also clamped on one section of the slide to provide an internal control. The sample collection time for data reported here was three weeks to meet the sensitivity limitations of the analytical techniques. The campaign took place between May 12 and June 1, 2020, but we include only a subset of samples herein. See campaign information in the ESI† for additional details regarding the sampling and post-sampling procedures. Participants recorded their daily cooking and cleaning activities and ambient conditions in a field diary. Clear trends were not observed between spectra and cooking type or frequency. After sampling was complete, samples were stored in glass containers at ambient conditions until analysis. Surface and particle morphology can be modified by refrigeration and/or freezing, as shown in Laskina *et al.*, so samples were kept at room temperature to best preserve these properties.[28]

Raman microspectroscopy

Microscope slides were analyzed between August 2020 and March 2021 using a Raman microspectrometer (LabRAM HR Evolution, HORIBA, Ltd) at ambient relative humidity (RH) (30–40%) and temperature (25 °C). The Raman spectrometer was equipped with a confocal optical microscope (100× SLMP long working distance Olympus objective, 0.9 numerical aperture). An 1800 groove per mm diffraction grating was used with the 800 mm length spectrograph (spectral range 400–1100 nm), and a CCD detector (1 inch, 1024 × 256 pixels, 26 μm^2 pixel size). A 532 nm Nd:YAG laser source (32 mW) with a spot size of 700 nm was operated with a neutral density filter allowing for 100% transmission. This yielded ~0.7 cm^{-1} spectral resolution at 532 nm with spectral resolution referring to dispersion per pixel

for the CCD. Initial calibration of the Raman instrument involved nine different frequencies,[29] some of which included the laser line at 532 nm (0 cm^{-1} shift), the Si wafter at 520 cm^{-1}, a calibration standard at 1004 cm^{-1}, and a diamond band at 1332 cm^{-1}, as well as calibration standards at higher frequencies to cover the full spectral window (up to 4000 cm^{-1}). Daily calibrations for the Raman spectrometer were conducted every 24 hours using the silicon wafer standard against the Stokes Raman signal of pure Si at 520 cm^{-1}.[30] Spot checks of known standards with higher frequency features (C–H and O–H stretching region) confirm the calibration has held steady with consistent values for years.[31,32] Sample spectra were collected with three accumulations at 15 s acquisition times from 500–4000 cm^{-1}. The experimental Raman spectra shown in the subsequent figures are each an average of 5 spectra and normalized by the quartz mode at 800 cm^{-1}. Five locations were analyzed on most samples (minimum three), though many did not have signal beyond the glass substrate.

O-PTIR spectroscopy

Optical photothermal infrared (O-PTIR) spectroscopy was also used to analyze the slides between February and April 2021. The mIRage infrared + Raman microscope (Photothermal Spectroscopy Corp.) consisted of a visible objective (4×, 0.13 numerical aperture, 17.3 mm working distance, Nikon Plan Fluor), a Cassegrain reflective objective for simultaneous use of IR and visible lasers (40×, 0.78 numerical aperture, 8.3 mm working distance, 55 μm × 42 μm field of view) and a QCL laser that covers 880 to 1950 cm^{-1}. This instrument has recently been developed and used to characterize submicron aerosol particles without contacting the sample.[33] The instrument and theory have been described in detail in a previous study.[34] For this application, IR spectra were collected at a scan rate of 100 cm^{-1} s^{-1} for 15 s acquisitions and averaged over 3 accumulations. The IR laser repetition rate was set at 100 kHz and 300 ns per pulse, and the IR power and visible laser were set to approximately 4–10 mW each. An average of 10 spectra were collected for each sample.

3-D profilometry

Slides were also analyzed using a 3D optical microscope (Bruker ContourGT, 130 nm lateral and better than 1 nm height resolution) at ambient RH and temperature in summer 2021. To establish the utility of this instrument for indoor surface film and particle analysis, it has been used to characterize the morphology of thin squalene and skin oil films deposited on silica.[35,36] This non-contact method allows for morphological characterization of organic materials that would otherwise accumulate on an AFM tip and introduce noise. Images were collected at 5× magnification over a 1200 μm × 800 μm area. 3D images were processed using Profilm Online.

Results and discussion

The ability to collect simultaneous samples from a range of dwellings and geographic regions provided a unique opportunity to gain insight into the variability of samples between and within occupied apartments and detached houses. Identical sampling methods were utilized across locations (Fig. 1a), with glass microscope slides oriented vertically and deployed in the habituated dwelling to act as passive samplers. The cover slide obscured part of the microscope slide from indoor air during sampling, which allowed for an internal blank for reference. Many households across the United States participated in this study, but we focus on 7 households that have broadly been categorized by geographical region: West, Midwest, and East. In each household, the glass slides were required to be placed in kitchens, and four households collected additional slides in other room types throughout the home.

Fig. 2 clearly shows that samples did not display a uniform coating, even in the kitchen where deposition is expected to occur the most rapidly due to high concentrations of aerosols associated with cooking.[20] For all samples, distinct particles or agglomerations were observed without clear accumulation of even layers. However, within the uneven nature of the deposition onto the slides, there was variation in the visibly apparent morphology. The top row of samples (Midwest3, West2, and Midwest1) all appear to have initially had liquid material deposit onto the slides, while other samples had what appear to be solid samples (Midwest2) or samples that deposited and were then coated or dried in an atypical manner (Midwest4 and East2). It is notable that even in these two images where a coating is observed on some particles, that non-coated particles are still observed and the morphology of the coated particle is very uneven, which is not indicative of a smooth

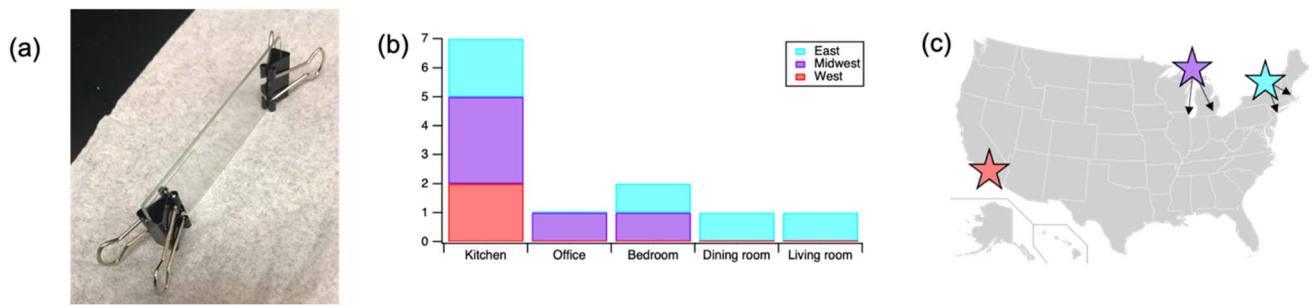

Fig. 1 Depiction of sampling method (a) and of room count (b) and geographical (c) locations. Samples were collected in three regions: East (blue), Midwest (purple), and West (red) in a variety of room types.

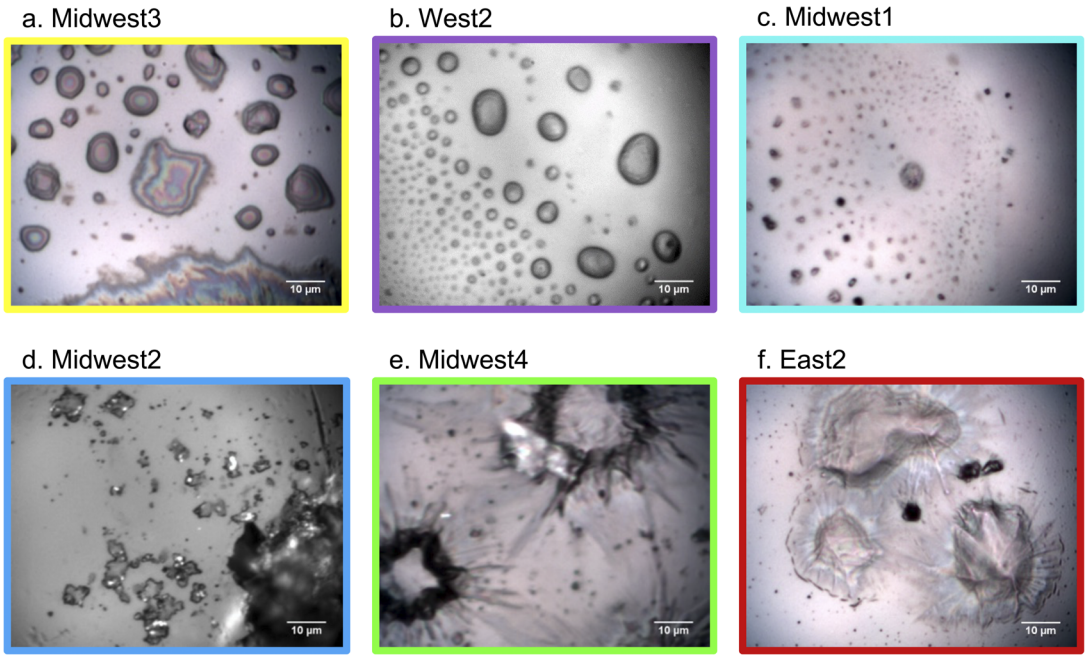

Fig. 2 Representative optical microscopy images of the glass substrate surfaces using a 100× objective (0.9 N.A.) on an Olympus microscope to characterize deposition from select kitchen samples: (a) Midwest3, (b) West2, (c) Midwest1, (d) Midwest2, (e) Midwest4, (f) East2.

homogeneous film growing on the substrate. This demonstrates a range of phase states within deposited particles.

Within the liquid-deposited samples, Midwest3 is likely composed of an oil, such as cooking oil, based on the multi-color appearance of the optical image. West2 appeared to be droplet-like, whereas Midwest1 may have been deposited as a droplet, but then dried. This highlights that even for liquid deposited samples, the RH and temperature of the dwelling will vary the properties of the available surfaces for future partitioning and multiphase chemistry. The more solid, almost crystalline, structure of particles deposited in the Midwest2 sample suggests a particle that was deposited as a solid, meaning it is less likely to have been an oil or other organic liquid that would not crystallize under typical indoor conditions. Midwest4 and East2 are much more unique in their appearance, with an apparent core particle that is coated with an organic film that has the appearance of biological material.

Recall the dichotomy in previous studies between: (1) studies having focused on particles deposited to a surface with unique morphology and chemical characteristics[20] and (2) studies that have focused on a model of a flat surface formed *via* more even deposition layers.[5,12,37] Further complicating matters for the first category of studies is that the phase of particles and films is variable, which can limit uptake by forming viscous crusts, as highlighted in Zhou *et al.*[38] From Fig. 2 the available surface for heterogeneous chemistry for these samples will likely be based upon the composition and phase state (*i.e.*, viscosity-based diffusion rate) of the film and less influenced by the particles underneath the coating.[39] This highlights the importance of microscopic characterization, as bulk analysis of these samples in isolation would include the coated components of East2 and Midwest4, which might be less important for overall partitioning and reactivity. The variety of morphologies suggests different sources as well as conditions, such as RH or temperature, during sampling (and storage).[28]

To more thoroughly characterize the glass substrate surface and heights of the particles observed in Fig. 2, the East1 kitchen sample was characterized with 3-D profilometry. The non-contact, optical surface profiles in Fig. 3 show how deposition accumulated in the East1 kitchen between one day and three weeks. After one day of sampling, Fig. 3a, there are initially some discrete particles on a relatively sparse background. After three weeks of sampling, Fig. 3b, not only does the vertical scale increase twofold, but many islands are observed. However, the formation of a relatively smooth layer is not observed. This is further highlighted in Fig. S1,† which shows line profiles from Fig. 3b. Surface topology is defined by deposited particles more so than films that grow evenly over this time scale, which is also in agreement with many outdoor studies.[40,41]

Much of the published research on surface properties in indoor dwellings has focused on kitchens, due to high emissions from cooking. Far fewer studies have investigated room-to-room variability of individual particles on surfaces,[6,7,19] and very few within inhabited dwellings. Fig. 4a shows the approximate layout of the dwelling East1, a compact apartment in a dense urban area, in which samples were collected in three adjacent rooms: the dining room (blue), kitchen (green), and bedroom (orange). The optical images (lower left) show that samples are likely deposited as liquids in the kitchen, but the more solid appearances of particles in the dining room and bedroom indicates either drying (*i.e.*, efflorescence) of particles transported from the kitchen or different sources of solid particles. Considering sampling was in springtime, the ambient atmosphere likely had abundant aerosol liquid water, further

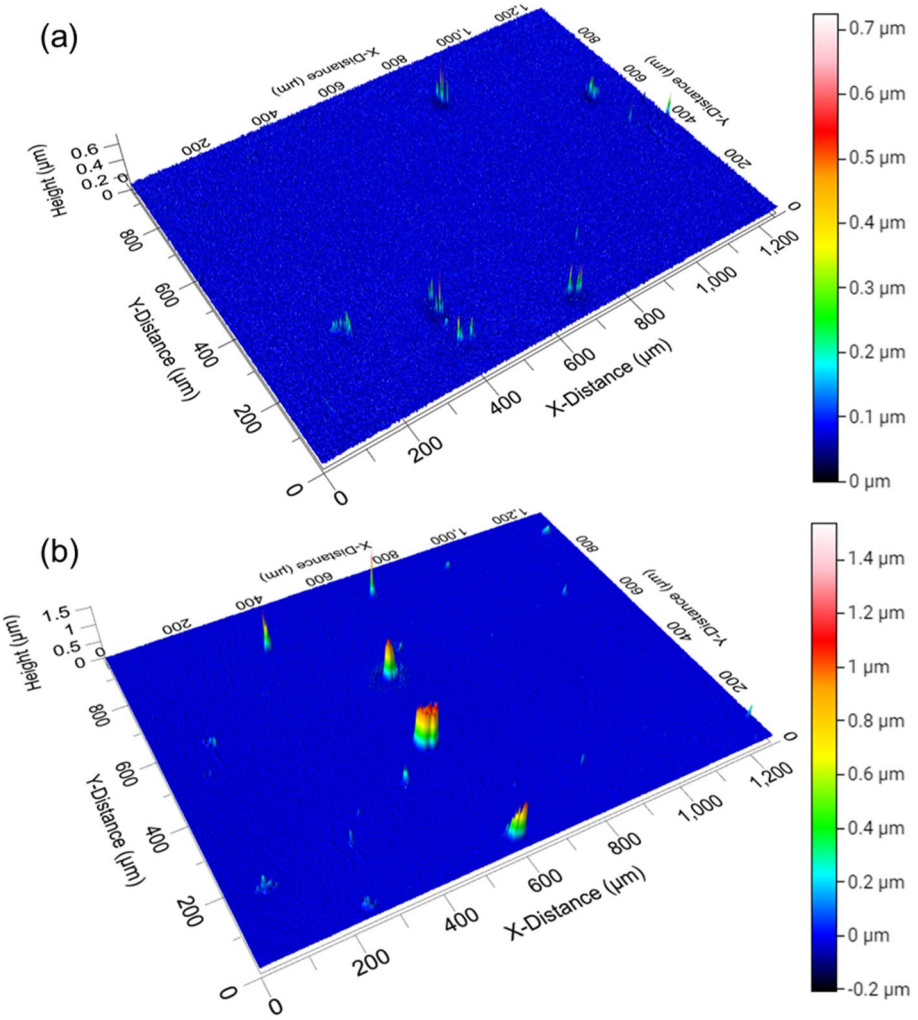

Fig. 3 3-D profilometry images from site East1 kitchen collected after 1 day (a) and 3 weeks (b).

highlighting that either particles were emitted as solids or solidified after transport indoors. To characterize these samples further, Raman spectra of the three-week samples are shown in Fig. 4b with the same color scheme as Fig. 4a. The majority of spectra for the dining room and bedroom samples had negligible signal, which was nearly identical to that of a clean glass slide (gray),[42] despite the presence of visible particles, which indicate less material or Raman-active species present. This background spectrum is representative of the internal blank for all of the samples. Spectra from kitchen samples had much more intensity and variation, with large signals in the C–H stretching region (shaded), indicating the presence of organic species.[43] Even within a single room, the particle morphology varies greatly, as shown in images of the kitchen slide in Fig. S2.† For the few samples with significant signal in the bedroom, the fingerprint region shows clear differences from the kitchen. For example, the C–H stretching region of the bedroom sample with higher peak intensity is quite distinct from both the C–H stretching region of particles collected in the kitchen and dining room. This suggests additional sources, phase changes, or continuing chemistry for particles between the different rooms. Thus, within this dwelling, there is likely either low air exchange between the rooms or a significant transformation as the particles are transported to different rooms throughout the dwelling.

Spectra collected from samples located in non-kitchen rooms are given in Fig. 5. The selected Raman spectra in Fig. 5a are the spectra with the most intense signals and show some commonalities for similar room types. This variability in spectra likely indicate a heterogeneous set of sources for these particles, which could be a mixture of indoor and outdoor sources. It should be noted that it was more difficult to locate particles and obtain spectra as the non-kitchen samples had less visible accumulation than many of the kitchen samples, which is in line with prior studies.[20] Nevertheless, the O-PTIR data in Fig. 5b shows an example of a particle from the Midwest4 living room that had limited Raman peaks, likely due to few strongly active Raman modes, but multiple IR modes that are strongly absorbing. Peaks in this spectrum are tentatively assigned as nitrate $\nu_{as}(NO_3^-)$ at 1361 cm^{-1}, ν(C=C) at 1593 cm^{-1}, and a carbonyl or ester ν(C=O) at 1753 cm^{-1}, indicating a particle with inorganic and organic components

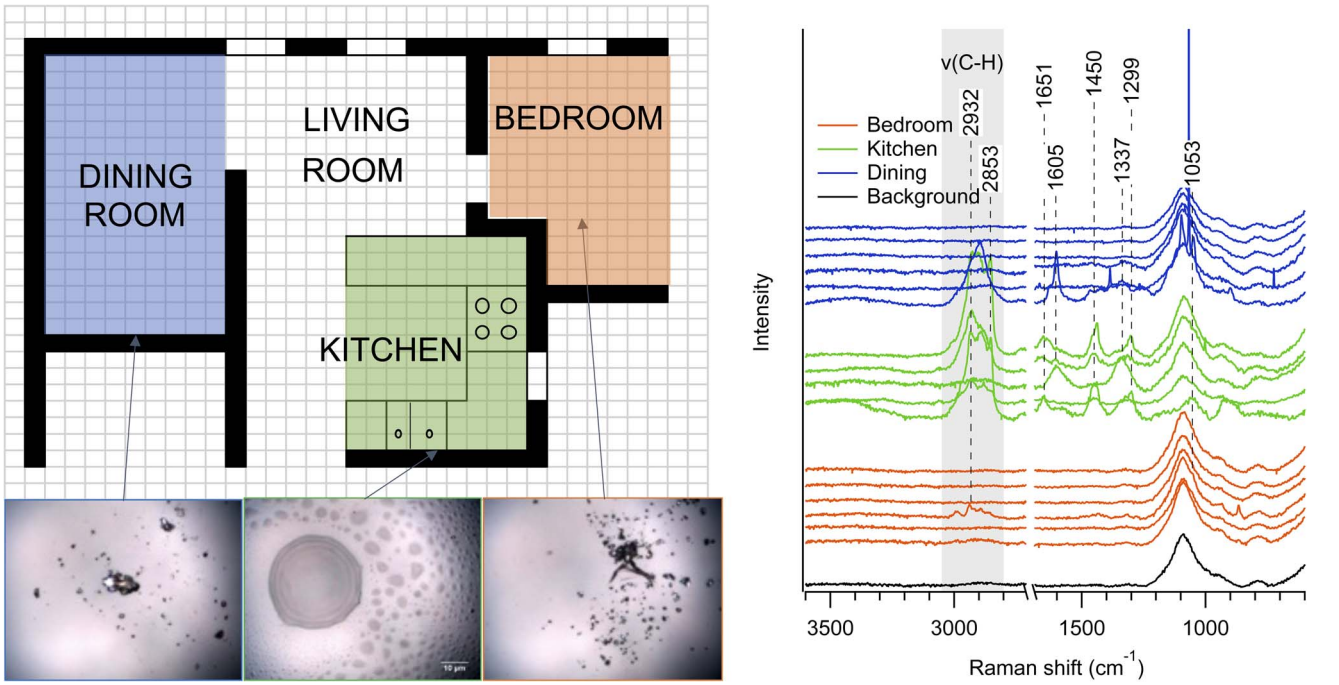

Fig. 4 Samples from adjacent rooms in a single household, East1, collected over three weeks. An approximate floorplan (a) highlights the rooms in which samples were collected and shows example images of some particles. Representative Raman spectra are shown panel (b) with the C–H stretching region highlighted with a gray box. The peak around 1100 cm^{-1} is from the glass substrate and indicated with an asterisk.

and a mixture of organic functional groups. The typical Raman peak for nitrate $\nu_s(NO_3^-)$ (~1050–1065 cm^{-1}) is observed in a few spectra, though the intensity of the signal from the glass slide (Si–O stretches) dominates that region.[42]

Fig. 6 shows individual single-particle Raman spectra from 3-week kitchen samples in various homes across the country. The C–H stretching region is highlighted in light gray and shows strong signals for most households, which indicate the

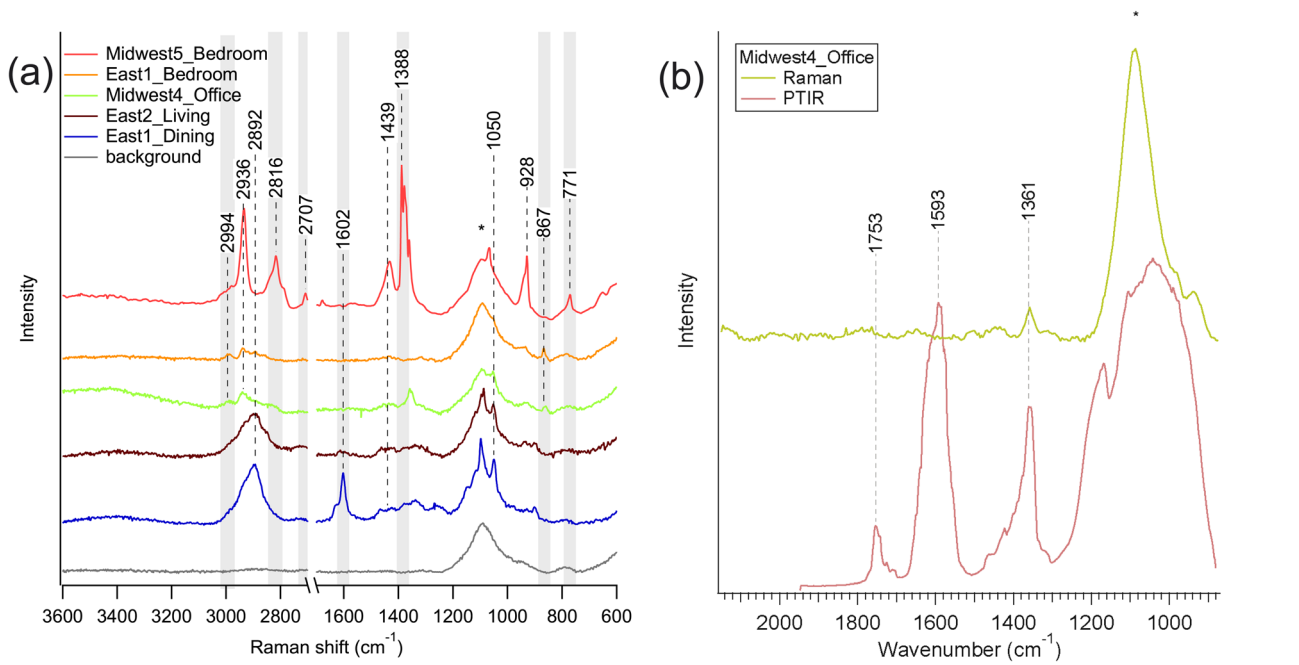

Fig. 5 (a) Raman spectra from non-kitchen rooms, and (b) a comparison of Raman (green) and O-PTIR (red) spectra for Midwest4 office (only sample in 5a with available O-PTIR spectra). The modes highlighted in light gray were not identified in kitchens, as shown below in Fig. 6. Note that the two East1 Raman spectra are the same as shown in Fig. 4. The peak around 1100 cm^{-1} is from the glass substrate and indicated with an asterisk, but peaks from the sample are visible on top of the broad feature of the glass peak.

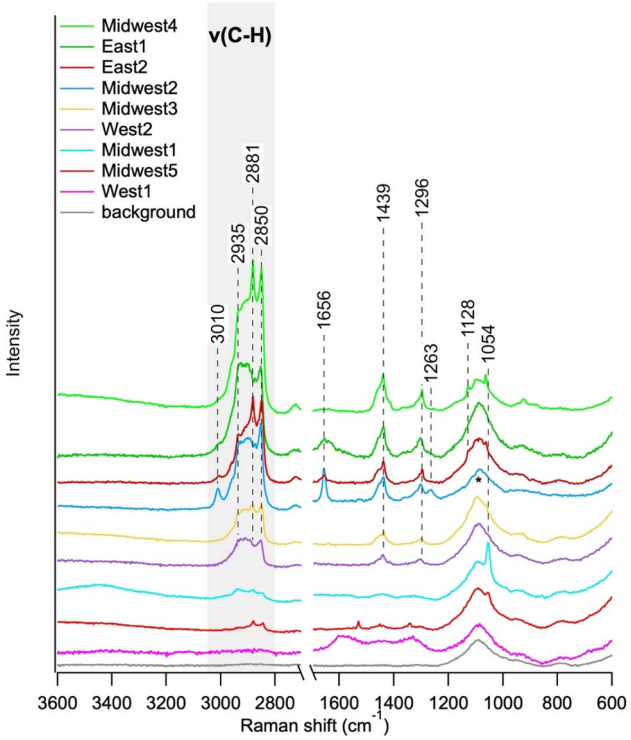

Fig. 6 Raman spectra from kitchens collected over 3 weeks. The gray box highlights the C–H stretching region. Note that the East1 Raman spectrum is the same as shown in Fig. 4. The peak around 1100 cm^{-1} is from the glass substrate and indicated with an asterisk.

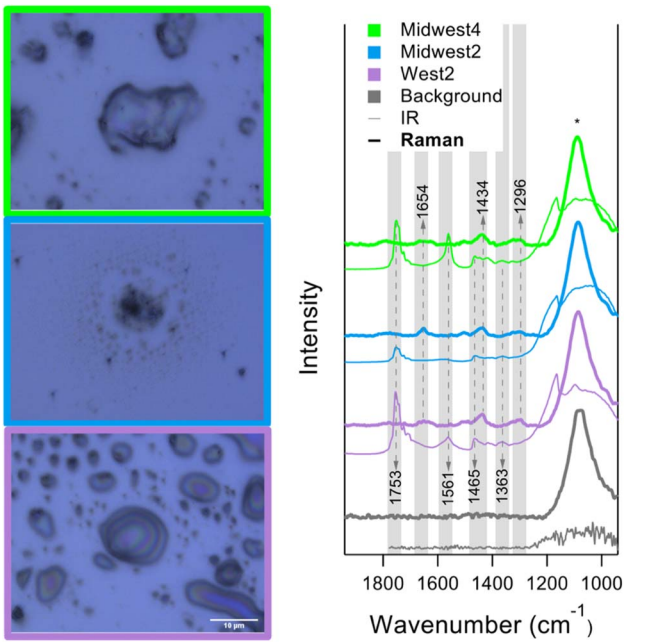

Fig. 7 O-PTIR (thin) and Raman (thick) spectra from select kitchens with representative images (Midwest4 – green, Midwest2 – blue, West2 – purple, glass slide – gray). The strongest modes are highlighted in grey, and the corresponding wavenumbers are labeled above for Raman spectra and below for IR spectra. The peak around 1100 cm^{-1} is from the glass substrate and indicated with an asterisk.

presence of organic material. The spectra from Midwest4 (light green) and East1 (dark red) show strong peaks for $\nu_s(CH_2)$ and $\nu_s(CH_3)$ relative to the other spectra, likely indicating long chain aliphatics.[44–46] Other spectra have greater intensity in higher frequency ν(C–H) modes indicating greater aromaticity.[43,44] The spectra from Midwest1 (turquoise), Midwest5 (red), and West1 (magenta) had less-intense organic features. This could be due to sample placement within the kitchen, proximity to the stove top, ventilation in the kitchen, cooking styles, food types, or a combination of these factors. Although organic compounds and particles are present in most of the kitchens, there is clearly heterogeneity between kitchens, which is unsurprising given the different cooking activities across kitchens.

To investigate the source and nature of these organic compounds, we looked at a pure canola oil sample from the home of Midwest2, as shown in Fig. S3.† The Midwest2 single-particle and canola oil spectra from the cooking spray used in Midwest2 are nearly identical. This was also consistent with the canola oil spectrum from Wiley's KnowItAll Spectral Library,[47] strongly indicating that the particle analyzed in Midwest2 is likely a canola oil droplet.

O-PTIR spectra from three kitchens are shown on the right-hand side of Fig. 7. Each spectrum is averaged from over 10 distinct points. Example images are shown on the left with the borders corresponding to the legends in the plot. From the images, the samples have a notable range in particle morphology and the structures likely indicate differences in organic phase as well. The thicker lines represent the Raman spectra, and the thinner lines represent the IR spectra. The Raman spectra are consistent with the spectra in Fig. 6. However, there are some consistent, strong IR modes that are Raman inactive, such as 1753 cm^{-1}, from carbonyl or ester stretching. This mode is also identified in the office of Midwest4, as shown in Fig. 5b.

Conclusion

A wide range of chemical and morphological heterogeneity was observed across rooms within a single dwelling, as well as between dwellings. In no dwelling were samples observed without significant contributions from particle deposition, which means that smooth films were not observed for the time period examined. This indicates that available surface area in these dwellings is likely strongly influenced by 3-dimensional surface features and particle deposition on the timescale of this sample collection. Or *et al.* showed previously substantial increases in surface area (~1–3 μm^2) from atomic force microscopy (AFM) of indoor samples, as well as surface coverages of 6–19%, for one day experiments and are likely in rough agreement with the samples discussed herein.[20] From chemical analysis, spectra from kitchens had relatively high intensities and clear contributions from organic particles, while particles in other rooms had notably different spectra and a higher fraction of solid particles. Not only were there differences between homes as might be expected, but more importantly there were stark differences between rooms within the same

dwelling and even between particles on a single substrate deployed in a single room. This is important as it highlights that sources, ventilation, and air flow patterns lead to distinct physical and chemical properties of surfaces even in a relatively compact dwelling. These examples from real-world dwellings add a layer of complexity when attempting to generalize and model indoor deposition. This work highlights the need to further understand heterogeneities of indoor surfaces to better understand the relative contribution of particles and thin film surface chemistry.

Data availability

Data for this article, including 2D images and micro-spectroscopic data, are available on the Deep Blue repository operated by the University of Michigan at **https://doi.org/10.7302/87tz-8w12**. 3D images are available at ProfilmOnline at **https://www.profilmonline.com/shared-folder?token=Rt6DwZTXWPv8**.

Conflicts of interest

There are no conflicts of interest to declare.

Acknowledgements

Funding for this work was provided by the Alfred P. Sloan Foundation through the Chemistry of Indoor Environments (CIE) program, specifically the SURFace consortium for the CIE program (SURF-CEI) through grant G-2019-12365, as well as individual grants: Prof. Ault (G-2018-11239), Prof. Grassian (G-2020-12675), Prof. Geiger (G-2019-12300), Prof. McNeill (G-2018-11032), and Prof. O'Brien (G-2018-11031 and G-2020-13953). This work also made use of the Keck-II and SPID facility of Northwestern University's NUANCE Center, which has received support from the SHyNE Resource (NSF ECCS-2025633), the International Institute for Nanotechnology (IIN), and Northwestern's MRSEC program (NSF DMR-1720139). Dr Victor Or is acknowledged for assistance with sample collection in San Diego. Dr Paula Olsiewski is gratefully acknowledged for guidance of the CIE program at the Alfred P. Sloan Foundation that supported this work. Dr Charles Weschler is thanked for helpful conversations and feedback. Prof. Delphine Farmer is acknowledged for feedback when initially formulating the Stay-At-HomeChem Field Manual.

References

1 J. D. Spengler and K. Sexton, Indoor air pollution: a public health perspective, *Science*, 1983, **221**(4605), 9–17.
2 J. González-Martín, N. J. R. Kraakman, C. Pérez, R. Lebrero and R. Muñoz, A state–of–the-art review on indoor air pollution and strategies for indoor air pollution control, *Chemosphere*, 2021, **262**, 128376.
3 N. E. Klepeis, W. C. Nelson, W. R. Ott, J. P. Robinson, A. M. Tsang, P. Switzer, J. V. Behar, S. C. Hern and W. H. Engelmann, The National Human Activity Pattern Survey (NHAPS): a resource for assessing exposure to environmental pollutants, *J. Expo. Anal. Environ. Epidemiol.*, 2001, **11**(3), 231–252.
4 J. P. D. Abbatt and D. B. Collins, Indoor Air Quality Through the Lens of Outdoor Atmospheric Chemistry, *Handbook of Indoor Air Quality*, 2021.
5 J. P. D. Abbatt and C. Wang, The atmospheric chemistry of indoor environments, *Environ. Sci.: Processes Impacts*, 2020, 25–48.
6 D. K. Farmer, M. E. Vance, J. P. D. Abbatt, A. Abeleira, M. R. Alves, C. Arata, E. Boedicker, S. Bourne, F. Cardoso-Saldaña, R. Corsi, P. F. DeCarlo, A. H. Goldstein, V. H. Grassian, L. Hildebrandt Ruiz, J. L. Jimenez, T. F. Kahan, E. F. Katz, J. M. Mattila, W. W. Nazaroff, A. Novoselac, R. E. O'Brien, V. W. Or, S. Patel, S. Sankhyan, P. S. Stevens, Y. Tian, M. Wade, C. Wang, S. Zhou and Y. Zhou, Overview of HOMEChem: House Observations of Microbial and Environmental Chemistry, *Environ. Sci.: Processes Impacts*, 2019, **21**(8), 1280–1300.
7 D. K. Farmer, M. E. Vance, D. Poppendieck, J. Abbatt, M. R. Alves, K. C. Dannemiller, C. Deeleepojananan, J. Ditto, B. Dougherty, O. R. Farinas, A. H. Goldstein, V. H. Grassian, H. Huynh, D. Kim, J. C. King, J. Kroll, J. Li, M. F. Link, L. Mael, K. Mayer, A. B. Martin, G. Morrison, R. O'Brien, S. Pandit, B. J. Turpin, M. Webb, J. Yu and S. M. Zimmerman, The chemical assessment of surfaces and air (CASA) study: using chemical and physical perturbations in a test house to investigate indoor processes, *Environ. Sci.: Processes Impacts*, 2025, DOI: **10.1039/D4EM00209A**.
8 G. Bekö, P. Wargocki, N. Wang, M. Li, C. J. Weschler, G. Morrison, S. Langer, L. Ernle, D. Licina, S. Yang, N. Zannoni and J. Williams, The Indoor Chemical Human Emissions and Reactivity (ICHEAR) project: Overview of experimental methodology and preliminary results, *Indoor Air*, 2020, **30**(6), 1213–1228.
9 D. K. Farmer, M. E. Vance, J. P. D. Abbatt, A. Abeleira, M. R. Alves, C. Arata, E. Boedicker, S. Bourne, F. Cardoso-Saldaña, R. Corsi, P. F. DeCarlo, A. H. Goldstein, V. H. Grassian, L. Hildebrandt Ruiz, J. L. Jimenez, T. F. Kahan, E. F. Katz, J. M. Mattila, W. W. Nazaroff, A. Novoselac, R. E. O'Brien, V. W. Or, S. Patel, S. Sankhyan, P. S. Stevens, Y. Tian, M. Wade, C. Wang, S. Zhou and Y. Zhou, Overview of HOMEChem: House Observations of Microbial and Environmental Chemistry, *Environ. Sci.:Processes Impacts*, 2019, **21**(8), 1280–1300.
10 A. Manuja, J. Ritchie, K. Buch, Y. Wu, C. M. A. Eichler, J. C. Little and L. C. Marr, Total surface area in indoor environments, *Environ. Sci.: Processes Impacts*, 2019, **21**(8), 1384–1392.
11 A. T. Hodgson, K. Y. Ming and B. C. Singer, *Quantifying Object and Material Surface Areas in Residences*, 2005.
12 C. Wang, D. B. Collins, C. Arata, A. H. Goldstein, J. M. Mattila, D. K. Farmer, L. Ampollini, P. F. DeCarlo, A. Novoselac, M. E. Vance, W. W. Nazaroff and J. P. D. Abbatt, Surface reservoirs dominate dynamic gas-

surface partitioning of many indoor air constituents, *Sci. Adv.*, 2020, eaay8973.
13 F. X. Mueller, L. Loeb and W. H. Mapes, Decomposition rates of ozone in living areas, *Environ. Sci. Technol.*, 1973, **7**(4), 342–346.
14 B. C. Singer, A. T. Hodgson, T. Hotchi, K. Y. Ming, R. G. Sextro, E. E. Wood and N. J. Brown, Sorption of organic gases in residential rooms, *Atmos. Environ.*, 2007, **41**(15), 3251–3265.
15 P. F. DeCarlo, A. M. Avery and M. S. Waring, Thirdhand smoke uptake to aerosol particles in the indoor environment, *Sci. Adv.*, 2018, **4**(5), eaap8368.
16 Y. Fang, S. Riahi, A. T. McDonald, M. Shrestha, D. J. Tobias and V. H. Grassian, What Is the Driving Force behind the Adsorption of Hydrophobic Molecules on Hydrophilic Surfaces?, *J. Phys. Chem. Lett.*, 2019, **10**(3), 468–473.
17 Y. Fang, P. S. J. Lakey, S. Riahi, A. T. McDonald, M. Shrestha, D. J. Tobias, M. Shiraiwa and V. H. Grassian, A molecular picture of surface interactions of organic compounds on prevalent indoor surfaces: limonene adsorption on SiO2, *Chem. Sci.*, 2019, **10**(10), 2906–2914.
18 A. P. Ault, V. H. Grassian, N. Carslaw, D. B. Collins, H. Destaillats, D. J. Donaldson, D. K. Farmer, J. L. Jimenez, V. F. McNeill, G. C. Morrison, R. E. O'Brien, M. Shiraiwa, M. E. Vance, J. R. Wells and W. Xiong, Indoor Surface Chemistry: Developing a Molecular Picture of Reactions on Indoor Interfaces, *Chem*, 2020, 3203–3218.
19 R. E. O'Brien, Y. Li, K. J. Kiland, E. F. Katz, V. W. Or, E. Legaard, E. Q. Walhout, C. Thrasher, V. H. Grassian, P. F. DeCarlo, A. K. Bertram and M. Shiraiwa, Emerging investigator series: chemical and physical properties of organic mixtures on indoor surfaces during HOMEChem, *Environ. Sci.:Processes Impacts*, 2021, **23**(4), 559–568.
20 V. W. Or, M. Wade, S. Patel, M. R. Alves, D. Kim, S. Schwab, H. Przelomski, R. O'Brien, D. Rim, R. L. Corsi, M. E. Vance, D. K. Farmer and V. H. Grassian, Glass surface evolution following gas adsorption and particle deposition from indoor cooking events as probed by microspectroscopic analysis, *Environ. Sci.: Processes Impacts*, 2020, **22**, 1698–1709.
21 W. D. Fahy, F. Wania and J. P. D. Abbatt, When Does Multiphase Chemistry Influence Indoor Chemical Fate?, *Environ. Sci. Technol.*, 2024, **58**(9), 4257–4267.
22 D. M. Lunderberg, K. Kristensen, Y. Tian, C. Arata, P. K. Misztal, Y. Liu, N. Kreisberg, E. F. Katz, P. F. DeCarlo, S. Patel, M. E. Vance, W. W. Nazaroff and A. H. Goldstein, Surface Emissions Modulate Indoor SVOC Concentrations through Volatility-Dependent Partitioning, *Environ. Sci. Technol.*, 2020, 6751–6760.
23 V. W. Or, M. R. Alves, M. Wade, S. Schwab, R. L. Corsi and V. H. Grassian, Crystal Clear? Microspectroscopic Imaging and Physicochemical Characterization of Indoor Depositions on Window Glass, *Environ. Sci. Technol. Lett.*, 2018, **5**(8), 514–519.
24 C. Y. Lim and J. P. Abbatt, Chemical Composition, Spatial Homogeneity, and Growth of Indoor Surface Films, *Environ. Sci. Technol.*, 2020, **54**(22), 14372–14379.
25 Z. Zhou, L. R. Crilley, J. C. Ditto, T. C. VandenBoer and J. P. Abbatt, Chemical fate of oils on indoor surfaces: ozonolysis and peroxidation, *Environ. Sci. Technol.*, 2023, **57**(41), 15546–15557.
26 Z. Zhou, S. Zhou and J. P. D. Abbatt, Kinetics and Condensed-Phase Products in Multiphase Ozonolysis of an Unsaturated Triglyceride, *Environ. Sci. Technol.*, 2019, **53**(21), 12467–12475.
27 Y. Liu, A. G. Bé, V. W. Or, M. R. Alves, V. H. Grassian and F. M. Geiger, Challenges and Opportunities in Molecular-Level Indoor Surface Chemistry and Physics, *Cell Rep. Phys. Sci.*, 2020, **1**(11), 100256.
28 O. Laskina, H. S. Morris, J. R. Grandquist, A. D. Estillore, E. A. Stone, V. H. Grassian and A. V. Tivanski, Substrate-Deposited Sea Spray Aerosol Particles: Influence of Analytical Method, Substrate, and Storage Conditions on Particle Size, Phase, and Morphology, *Environ. Sci. Technol.*, 2015, **49**(22), 13447–13453.
29 Z. Lei, S. E. Bliesner, C. N. Mattson, M. E. Cooke, N. E. Olson, K. Chibwe, J. N. L. Albert and A. P. Ault, Aerosol Acidity Sensing via Polymer Degradation, *Anal. Chem.*, 2020, **92**(9), 6502–6511.
30 R. L. Craig, A. L. Bondy and A. P. Ault, Surface Enhanced Raman Spectroscopy Enables Observations of Previously Undetectable Secondary Organic Aerosol Components at the Individual Particle Level, *Anal. Chem.*, 2015, **87**(15), 7510–7514.
31 R. L. Craig, A. L. Bondy and A. P. Ault, Computer-controlled Raman microspectroscopy (CC-Raman): A method for the rapid characterization of individual atmospheric aerosol particles, *Aerosol Sci. Technol.*, 2017, **51**(9), 1099–1112.
32 A. M. Fankhauser, Z. Lei, K. R. Daley, Y. Xiao, Z. Zhang, A. Gold, B. S. Ault, J. D. Surratt and A. P. Ault, Acidity-Dependent Atmospheric Organosulfate Structures and Spectra: Exploration of Protonation State Effects via Raman and Infrared Spectroscopies Combined with Density Functional Theory, *J. Phys. Chem. A*, 2022, **126**(35), 5974–5984.
33 N. E. Olson, Y. Xiao, Z. Lei and A. P. Ault, Simultaneous Optical Photothermal Infrared (O-PTIR) and Raman Spectroscopy of Submicrometer Atmospheric Particles, *Anal. Chem.*, 2020, **92**(14), 9932–9939.
34 D. Zhang, C. Li, C. Zhang, M. N. Slipchenko, G. Eakins and J.-X. Cheng, Depth-resolved mid-infrared photothermal imaging of living cells and organisms with submicrometer spatial resolution, *Sci. Adv.*, 2016, **2**(9), e1600521.
35 M. von Domaros, Y. Liu, J. L. Butman, E. Perlt, F. M. Geiger and D. J. Tobias, Molecular Orientation at the Squalene/Air Interface from Sum Frequency Generation Spectroscopy and Atomistic Modeling, *J. Phys. Chem. B*, 2021, **125**(15), 3932–3941.
36 J. L. Butman, R. J. Thomson and F. M. Geiger, Unanticipated Hydrophobicity Increases of Squalene and Human Skin Oil Films Upon Ozone Exposure, *J. Phys. Chem. B*, 2022, **126**(45), 9417–9423.
37 C. J. Weschler and W. W. Nazaroff, Growth of organic films on indoor surfaces, *Indoor Air*, 2017, **27**(6), 1101–1112.

38 S. M. Zhou, M. Shiraiwa, R. D. McWhinney, U. Poschl and J. P. D. Abbatt, Kinetic limitations in gas-particle reactions arising from slow diffusion in secondary organic aerosol, *Faraday Discuss.*, 2013, **165**, 391–406.
39 S. Zhou, B. C. Hwang, P. S. Lakey, A. Zuend, J. P. Abbatt and M. Shiraiwa, Multiphase reactivity of polycyclic aromatic hydrocarbons is driven by phase separation and diffusion limitations, *Proc. Natl. Acad. Sci. U. S. A.*, 2019, **116**(24), 11658–11663.
40 J. L. DeYoung, U. G. Akporere, Z. Cheng, S. China, G. W. Vandergrift, C. R. Anderton, Y. Zhou, Z. Zhu and S. K. Shaw, Chemical Differences in Environmental Films Collected on Surfaces with Different Hydrophilicity, *ACS Earth Space Chem.*, 2024, **8**(12), 2411–2419.
41 C. R. Kroptavich, S. Zhou, S. F. Kowal and T. F. Kahan, Physical and Chemical Characterization of Urban Grime Sampled from Two Cities, *ACS Earth Space Chem.*, 2020, **4**(10), 1813–1822.
42 H. Liu, H. Kaya, Y. T. Lin, A. Ogrinc and S. H. Kim, Vibrational spectroscopy analysis of silica and silicate glass networks, *J. Am. Ceram. Soc.*, 2022, **105**(4), 2355–2384.
43 J. A. Mirrielees, R. M. Kirpes, S. M. Haas, C. D. Rauschenberg, P. A. Matrai, A. Remenapp, V. L. Boschi, A. M. Grannas, K. A. Pratt and A. P. Ault, Probing Individual Particles Generated at the Freshwater–Seawater Interface through Combined Raman, Photothermal Infrared, and X-ray Spectroscopic Characterization, *ACS Meas. Sci. Au*, 2022, **2**(6), 605–619.
44 A. P. Ault, D. F. Zhao, C. J. Ebben, M. J. Tauber, F. M. Geiger, K. A. Prather and V. H. Grassian, Raman microspectroscopy and vibrational sum frequency generation spectroscopy as probes of the bulk and surface compositions of size-resolved sea spray aerosol particles, *Phys. Chem. Chem. Phys.*, 2013, **15**(17), 6206–6214.
45 C. J. Ebben, A. P. Ault, M. J. Ruppel, O. S. Ryder, T. H. Bertram, V. H. Grassian, K. A. Prather and F. M. Geiger, Size-Resolved Sea Spray Aerosol Particles Studied by Vibrational Sum Frequency Generation, *J. Phys. Chem. A*, 2013, **117**(30), 6589–6601.
46 R. G. Snyder, H. L. Strauss and C. A. Elliger, C-H stretching modes and the structure of normal alkyl chains 1. long disordered chains, *J. Phys. Chem.*, 1982, **86**(26), 5145–5150.
47 Wiley Science Solutions, KnowItAll IR Spectral Database Collection, **https://sciencesolutions.wiley.com/solutions/technique/ir/knowitall-ir-collection/**.